

Magneto-convection around a pair of differentially heated pipes

C. COURTESSOLE^{1*}, L. BÜHLER¹, C. MISTRANGELO¹

¹ Karlsruhe Institute of Technology, Postfach 3640, 76021 Karlsruhe, Germany.

*Corresponding author: cyril.courtessole@kit.edu

Abstract: A parametric study was performed over a range of Grashof numbers $10^6 \leq Gr \leq 5 \cdot 10^7$ and Hartmann numbers $0 \leq Ha \leq 3000$. Depending on the strengths of buoyant and electromagnetic forces, several flow regimes were observed from recorded temperature data. The effect of the electromagnetic force primarily consists in suppressing turbulence and damping the convective flow. The heat transfer is quantified in terms of the nondimensional Nusselt number Nu , and its dependence on Gr/Ha^2 , which is identified as the important combined parameter governing the flow, is discussed. Experimental results are complemented by a 3D numerical analysis that sheds light on the flow structure that cannot be obtained from the experimental study.

Key words: Heat transfer, Liquid metal experiment, Numerical simulation, Magneto-convection

1. Introduction Magneto-convection occurs in buoyancy-driven liquid metal flows in the presence of magnetic fields. It has application in engineering fields, such as advanced material manufacturing, e.g., crystal growth of semiconductors [1] and nuclear fusion technology, where liquid metals serve for tritium self-sufficiency and power conversion [2]. Among liquid breeder blanket systems being developed for the latter application, the water-cooled lead-lithium (WCLL) concept, currently investigated as European reference design, may exhibit particularly strong magneto-convective effects [3]. In this blanket, the liquid metal is slowly circulated for tritium recovery with its forced flow reduced to a few mm/s to minimize magnetohydrodynamic (MHD) pressure drop. Heat extraction is achieved by water-cooled pipes immersed in the liquid metal leading to large thermal gradients within the fluid.

Besides the interest in the field of fusion engineering, heat transfer at horizontal pipes in a strong magnetic field constitutes a fundamental problem in magnetohydrodynamics. MHD heat transfer and, more generally, magneto-convection in pipes and ducts has been studied by many a number of authors and in several configurations, as is evident from the comprehensive review by Zikanov et al. [4]. However, geometries with internal obstacles, such as cooling pipes, have not attracted similar attention.

With the scope of investigating magneto-convective flows relevant to WCLL blankets, a generic model geometry has been selected for studying convective heat transfer between two differentially heated horizontal cylinders in a magnetic field. A parametric study was performed experimentally in the MEKKA laboratory at KIT and companion numerical simulations have been carried out to better understand typical flow patterns. Flows and associated heat transfer were analyzed and comparison between experimental and numerical results are discussed.

2. Definition of the problem The problem consists of a rectangular cavity formed by adiabatic and electrically insulated walls in which two parallel cylinders are inserted horizontally along the \hat{x} -direction (Figure 1). The directions of magnetic field

$\mathbf{B} = -B \hat{y}$ and gravity $\mathbf{g} = -g \hat{y}$ are aligned and anti-parallel to the y coordinate. The characteristic length of the geometry L is half the distance between the so-called Hartmann walls (HW), which are perpendicular to the applied magnetic field. For nondimensionalization, all lengths are scaled by L such that the liquid metal is confined to $-2 \leq x \leq 2$, $-1 \leq y \leq 1$, $-2 \leq z \leq 2$. Walls parallel to the magnetic field are referred to as end walls (EW) at $x = \pm 2$ and side walls (SW) at $z = \pm 2$. In the box-centered coordinate system, the axes of the cooled and heated cylinders are located at $y = 0$ and at $z = 1$ and $z = -1$, respectively, i.e., L is also a typical scale for the distance of the cylinders that is relevant for the driving horizontal temperature gradient. In this setup, the driving differential temperature $\Delta T = (T_2 - T_1) / 2$ is imposed by the two cylinders maintained at constant temperatures $T_1 = \bar{T} - \Delta T$ and $T_2 = \bar{T} + \Delta T$, where $\bar{T} = (T_1 + T_2) / 2$ is the mean temperature.

The nondimensional parameters quantifying the importance of the electromagnetic and buoyant effects are the Hartmann Ha and Grashof numbers Gr , respectively. More precisely, the ratio of electromagnetic to viscous forces is given by the square of Hartmann number, and the Grashof number denotes the ratio of buoyant and viscous force. The heat transfer at the pipes is defined in terms of the Nusselt number representing the ratio of convective heat transfer to pure heat conduction. These nondimensional numbers are expressed as follow:

$$Ha = BL \sqrt{\frac{\sigma}{\mu}}, Gr = \frac{g\beta\Delta TL^3}{\nu^2}, Nu = \frac{hL}{k}, \quad (1)$$

where h is the heat transfer coefficient. The thermophysical properties of the model fluid, a gallium-indium-tin alloy (GaInSn), i.e. density ρ , coefficient of volumetric thermal expansion β , kinematic viscosity ν , and thermal and electrical conductivities k and σ have been taken at the average temperature \bar{T} , set to 30 °C during the experiments, as reported in [5].

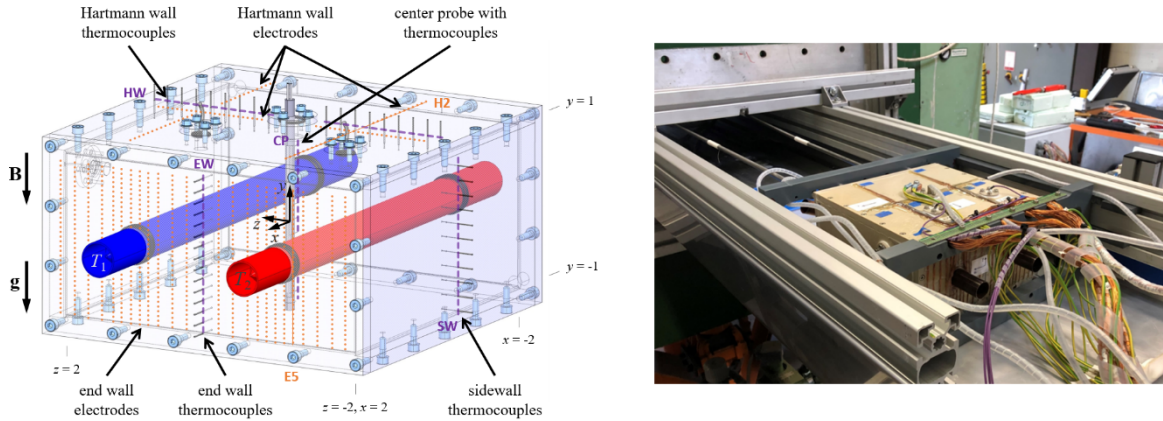


Figure 1. Geometry of the problem (left) and photo of the instrumented test section (right) installed on its levelling frame in front of the magnet in the MEKKA laboratory.

2.1 Numerical model The MHD flow in the rectangular cavity is governed by the conservation of momentum, energy, mass $\nabla \cdot \mathbf{v} = 0$ and charge $\nabla \cdot \mathbf{j} = 0$ that, combined with the Ohm's law $\mathbf{j} = \sigma (-\nabla\phi + \mathbf{v} \times \mathbf{B})$, lead to the set of equations:

$$\rho_0 \left(\frac{\partial}{\partial t} + \mathbf{v} \cdot \nabla \right) \mathbf{v} = -\nabla p + \rho_0 \nu \nabla^2 \mathbf{v} - \rho_0 \beta (T - \bar{T}) \mathbf{g} + \mathbf{j} \times \mathbf{B} \quad (2)$$

$$\rho_0 c_p \left(\frac{\partial T}{\partial t} + (\mathbf{v} \cdot \nabla) T \right) - k \nabla^2 T = 0 \quad (3)$$

$$\nabla^2 \phi = \nabla(\mathbf{v} \times \mathbf{B}) \quad (4)$$

Here, \mathbf{v} , \mathbf{j} , \mathbf{B} , p , T and ϕ refer to the velocity, current density, applied magnetic field, pressure, temperature and electric potential, and the Boussinesq approximation is used to

express the buoyancy force resulting from density variation with respect to the reference density $\rho_0 = \rho(\bar{T})$ caused by the nonuniform temperature distribution within the fluid.

No-slip boundary conditions ($\mathbf{v} = 0$) are imposed at the walls and, since all walls are thermally and electrically insulated, $\partial\phi/\partial n = 0$ and $\partial T/\partial n = 0$. The pipes are electrically insulating and isothermal with differential temperatures T_1 and T_2 .

Equations (2)–(4) have been implemented in the finite volume open source code OpenFOAM. A segregated method has been used to solve the problem. The solution of pressure and velocity is obtained by using preconditioned conjugate and biconjugate gradient solvers, respectively, and the Poisson equation is solved with an algebraic multigrid method for the electric potential. The Lorentz force is treated explicitly and defined at cell-centers with face current fluxes interpolated in divergence form by using the vector identity $\mathbf{j} = \nabla \cdot (\mathbf{j}\mathbf{r})$, where \mathbf{r} is the distance vector [6].

2.2 Experimental set-up A detailed description of the experimental set-up shown in Figure 1 can be found in [7]. The liquid metal is contained in a rectangular box measuring 200mm \times 100mm \times 200mm, such that the characteristic length of the problem is $L = 50$ mm. The test section is made of PEEK plastic and thermally insulated with polystyrene installed on its Hartmann walls and on all lateral walls. The two horizontal cylinders immersed in the liquid metal are inserted 100 mm apart and each copper pipe is connected to its own temperature-controlled water circuit, which includes a thermostat providing stable temperatures within ± 0.05 °C. The external surface of the tubes is coated with a 2 μ m thick silicon carbide layer to prevent corrosion from the liquid metal. This layer is thin enough for its thermal resistance to be neglected and provides electrical insulation of the pipes, hence avoiding thermoelectric effects at the copper/GaInSn interface.

The test section is equipped with 55 copper-constantan thermocouples and 414 copper electrodes to measure both temperature and electric potential. Temperatures are measured along the magnetic field direction at the middle of an EW at $(2, y, 0)$, on the SW closest to the hot pipe at $(x_p, y, -2)$ and close to the center of the cavity (CP) at $(x_p = -0.13, y, 0)$. In addition, thermocouples are installed at the top fluid/wall interface to capture the temperature distribution at the Hartmann wall along the direction orthogonal to the pipes $(x_p, 1, z)$. Electric potential is recorded above each pipe on the top Hartmann wall by two sets of electrodes at $(x, 1, 1)$ (H1) and $(x, 1, -1)$ (H2) and along the z -direction (H3) at $(0, 1, z)$. Furthermore, one end wall of the cavity ($x = 2$) is covered with 356 through electrodes. All potential signals are measured with respect to a reference electrode located at $z = 0$ on the top Hartmann wall. Finally, the amount of heat exchanged between the cylinders and the liquid metal is indirectly quantified by measuring the heat loss or gain by water at the hot or cooled pipe, respectively. To do so, each temperature-controlled circuit is equipped with a dedicated flowmeter that records the mass flowrate \dot{m} of water in the pipe, and a pair of thermocouple positioned upstream and downstream the inner cores assess the temperature variation ΔT_x along the pipe axes.

3. Results

3.1 Computed flow A detail description of the numerical computations can be found in [8]. Results obtained for $Gr = 2.5 \cdot 10^7$, i.e. for a characteristic temperature difference $\Delta T = 17.34$ K, and several Hartmann numbers ($Ha = 50, 500, \text{ and } 1000$) are shown in Figure 2 where contours of velocity magnitude and temperature are plotted. When a weak magnetic field is applied (Figure 2a), the flow exhibits a large-scale recirculation located between the cylinders. It is formed by a thermal plume that ascends around the warm pipe, impinges against the top wall of the cavity, and descends around the cold one. The flow is time-dependent and the boundary layers detach from the cylinders. It is characterized by a stable horizontal thermal stratification where hot layers of fluid sit on top of colder ones.

When the strength of the applied magnetic field increases (Figure 2b,c), the flow becomes stationary and the temperature contours progressively tilt as the convection cell is damped by more intense Lorentz forces. For large enough Hartmann numbers, isotherms become eventually vertical signaling that thermal conduction becomes the primary heat transfer mechanism. Most of the flowrate is now constraint to Ludford-like internal boundary layers tangent to the pipes and aligned with the magnetic field, whereas jet-like velocity profile with increased velocity occurs at the end walls of the enclosure, parallels to the direction of the applied magnetic field.

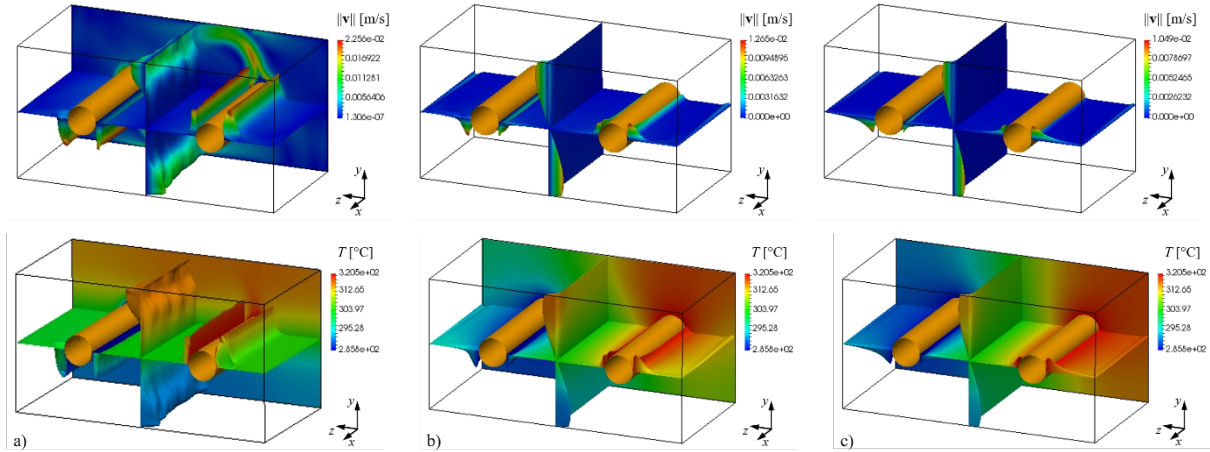


Figure 2. Magneto-convective flows at $Gr = 2.5 \cdot 10^7$ and $Ha = 50$ (a), 500 (b), and 1000 (c). Contours of velocity magnitude (top) and temperature (bottom) are shown in half geometry on horizontal ($y = 0$) and vertical ($z = 0$) middle planes.

3.2 Experimental results Magneto hydrodynamic experiments were performed for various magnetic fields ranging from 25 mT to 1.5 T, corresponding to $0 \leq Ha \leq 3000$, and for Grashof numbers in the range $10^6 \leq Gr \leq 5 \cdot 10^7$, i.e. for temperature differences $T_2 - T_1$ ranging from less than 2 °C to almost 70 °C. Results are presented in nondimensional notation where $T^* = (T - \bar{T}) / \Delta T$. For simplicity, the star notation is omitted in the rest of the text. Further details can be found in [7].

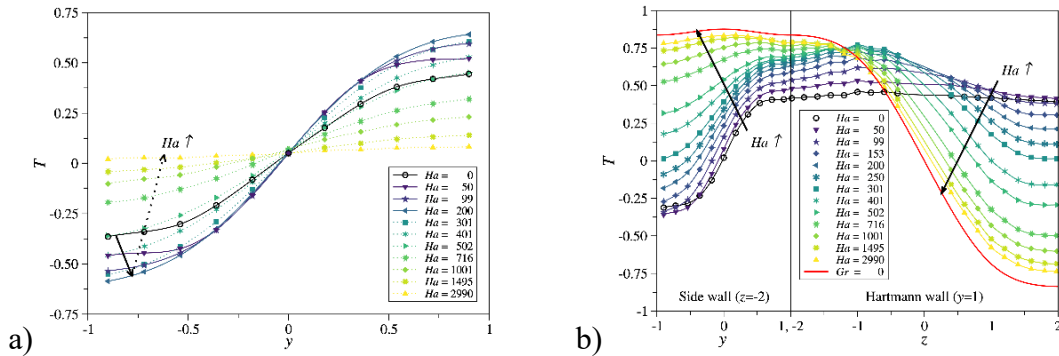


Figure 3. Nondimensional temperature distributions measured in the center (CP) of the cavity (a) and in the middle plane along the “hot” sidewall and the top Hartmann wall (b) for $Gr = 2.5 \cdot 10^7$ and $0 \leq Ha \leq 3000$. The solid red line represents a theoretical result for pure heat conduction with $Gr = 0$.

The magnetic damping of convection is illustrated by the results presented in Figure 3, obtained for $Gr = 2.5 \cdot 10^7$ and gradually increasing Hartmann numbers. As Ha increases, the temperature amplitude in the center of the cavity first grows to reach a maximum value for $Ha \approx 200$. This is evidence of the initial suppression of turbulence mixing in the hot and cold layers at moderate Hartmann numbers, which leads to a more pronounced thermal stratification. For

larger Hartmann numbers, the temperature gradient $\partial_y T(x_p, 0, 0)$ at the center of the cavity monotonically decreases since magnetic braking reduces the fluid velocity thereby significantly impeding convective heat transfer until eventually, for very large Ha , convective transport seemingly vanishes. As a result, for large Ha , isotherms become vertical in the center of the cavity. This behavior is confirmed by measurements on the wall-fluid interface shown in Figure 3b and in full agreement with numerical results presented in Figure 4.

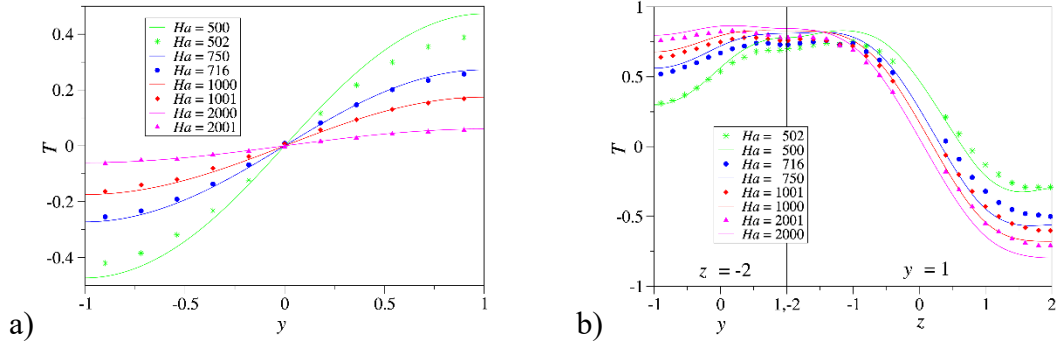


Figure 4. Comparison of calculated (solid lines) and measured (symbols) nondimensional temperature in the center of the cavity (a) and in the middle plane along the “hot” sidewall and the top Hartmann wall (b) for $Gr = 2.5 \cdot 10^7$ and several Hartmann numbers.

Computed electric potential cannot be directly compared with experimental data [9]. When comparing wall potential, it is necessary to recall that measurements include a flow-induced MHD contribution ϕ_{MHD} and a thermoelectric component ϕ_{TE} as voltages are measured between copper electrodes that are at different temperatures. Since the temperature field is known from numerical simulations in the entire cavity, and the Seebeck coefficient of couple GaInSn/Cu has been measured, it is possible to compute the thermoelectric contribution and to compare the total potential calculated $\phi = \phi_{MHD} + \phi_{TE}$ to experimental data. Results are shown for $Gr = 2.5 \cdot 10^7$ and $Ha = 2000$ on Figure 5. Here ϕ denotes nondimensional potential, i.e. potential normalized by $\phi_0 = u_0 BL$, with $u_0 = \rho_0 g \beta \Delta T / \sigma B^2$ being the characteristic velocity scale of the problem. Results are plotted along lines E5 and H2 on the end wall and the top Hartmann wall (see Figure 1). The axial profile (Fig. 5b) clearly highlights the strong contribution of the thermoelectric effect and shows that there is no flow-induced potential in the center of the cavity, whereas the convection motion near the end walls at $x = \pm 2$ generates a larger velocity-induced potential ϕ_{MHD} .

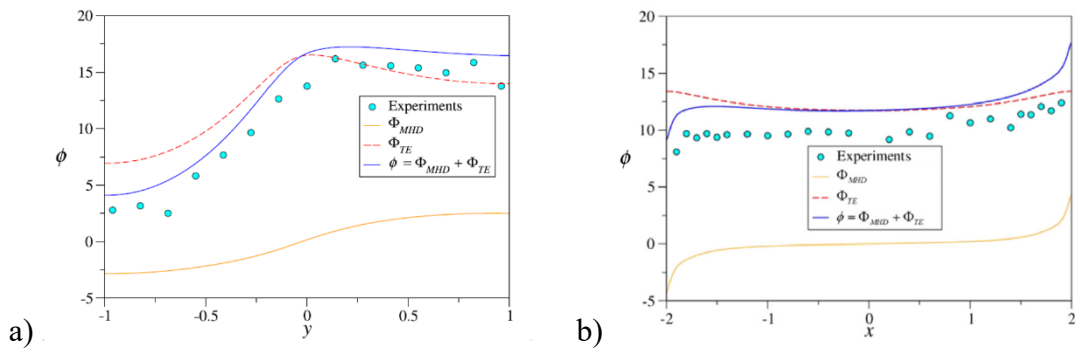


Figure 5. Experimental data (symbols) are compared with numerical results along the vertical line E5 on the end wall at $(2, y, -1.24)$ (a) and on the top Hartmann wall along line H2 above the hot pipe (b) for $Gr = 2.5 \cdot 10^7$ and $Ha = 2000$.

When comparing data obtained for various applied temperature differences, i.e. for different Gr , and growing Hartmann numbers, it clearly appears that it takes progressively stronger buoyancy forces to overcome the increasingly higher magnetic braking. The competition between the buoyancy force, promoting the convective flow, and the

electromagnetic force suppressing it is clearly highlighted in Figure 6. The results collected for different (Gr, Ha) demonstrate that the magneto-convective flow is controlled by a single similarity parameter since data collapse to unique distributions for the same quantity Gr/Ha^2 at all measurement locations.

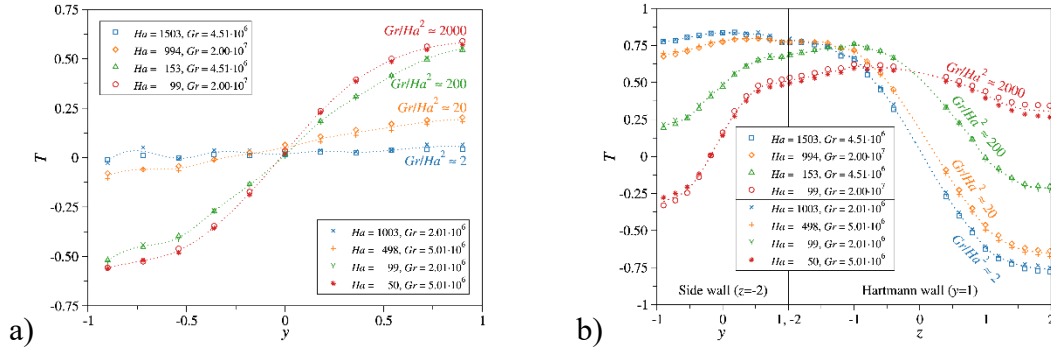


Figure 6. Nondimensional temperature distributions measured in the center of the cavity (CP) (a) and in the middle plane along the “hot” sidewall and the top Hartmann wall (b) for various Gr/Ha^2 .

The dependence of results on the combined parameter Gr/Ha^2 is also confirmed when plotting the Nusselt numbers in Figure 7, where several heat transfer regimes can be identified. At the lowest values of Gr/Ha^2 investigated, i.e., $Gr/Ha^2 \leq 10$, the purely conductive regime is confirmed since the Nusselt numbers approach a constant value close to $Nu_0 = 1.33$ given by the theoretical prediction. For $30 \leq Gr/Ha^2 \leq 500$, the heat transfer varies as $Nu \sim (Gr/Ha^2)^{1/5}$. Finally, as Gr/Ha^2 further increases, an inflection in Nu growth can be observed as the flow likely becomes turbulent in the layers near the end walls.

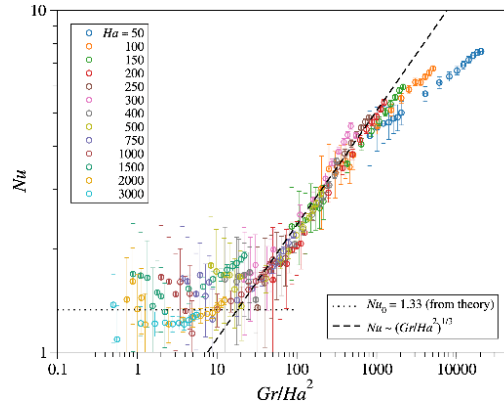


Figure 7. Nusselt numbers measured for various (Gr, Ha) .

4. Conclusions Magneto-convection around two differentially heated circular cylinders immersed in liquid metal that is confined in a rectangular cavity has been investigated. With increasing magnetic field, thin field-aligned layers develop tangentially to the cylinders and along vertical walls. While the convective flow in the core is strongly damped, some residual flow with associated heat transfer persists in thin layers along the end walls. Results show very good agreement between experimental and numerical data. The magneto-convective flow is controlled by the single combined parameter Gr/Ha^2 .

Acknowledgments This work has been carried out within the framework of the EUROfusion Consortium, funded by the European Union via the Euratom Research and Training Programme (Grant Agreement No 497 101052200 — EUROfusion). Views and opinions expressed are however those of the author(s) only and do not necessarily reflect those of the European Union or the European Commission. Neither the European Union nor the European Commission can be held responsible for them.

REFERENCES

- [1] H. OZOE. *Magnetic convection* (Imperial College Press, London, 2005).
- [2] G. FEDERICI, L. BOCCACCINI, F. CISMONDI, M. GASPAROTTO, Y. POITEVIN AND I. RICAPITO. An overview of the EU breeding blanket design strategy as an integral part of the DEMO design effort. *Fusion Engineering and Design*, 141, 30-42 (2019).
- [3] S. SMOLENTSEV, R. MOREAU, L. BÜHLER AND C. MISTRANGELO. MHD thermofluid issues of liquid-metal blankets: phenomena and advances. *Fusion Engineering and Design*, 85, 1196-1205 (2010).
- [4] O. ZIKANOV, I. BELYAEV, Y. LISTRATOV, P. FRICK, N. RAZUVANOV AND V. SVIRIDOV. Mixed convection in pipe and duct flows with strong magnetic fields. *Applied Mechanics Reviews*, 73, 010801 (2021).
- [5] Y. PLEVACHUK, V. SKLYARCHUK, S. ECKERT, G. GERBETH, AND R. NOVAKOVIC. Thermophysical properties of the liquid Ga-In-Sn eutectic alloy. *Journal of Chemical and Engineering Data*, 59, 757-763 (2014).
- [6] M.-J. NI, R. MUNIPALLI, N. MORLEY, P. HUANG AND M. ABDOU. A current density conservative scheme for incompressible MHD flows at low magnetic Reynolds number. Part I: On a rectangular collocated grid system. *Journal of Computational Physics*, 227, 174-204 (2007).
- [7] C. COURTESOLE, H.-J. BRINKMANN AND L. BÜHLER. Experimental investigation on magneto-convective flows around two differentially heated horizontal cylinders. *Journal of Fluid Mechanics*, in print (2024).
- [8] C. MISTRANGELO, L. BÜHLER, H.-J. BRINKMANN, C. COURTESOLE, V. KLÜBER AND C. KOEHLI. Magneto-convective flows around two differentially heated cylinders. *Heat and Mass Transfer*, vol. 59, 2005-2021 (2023).
- [9] C. MISTRANGELO, L. BÜHLER, C. COURTESOLE AND C. KOEHLI. Numerical and experimental analysis of magneto-convective flows around pipes. *Fusion Engineering and Design*, 202, 114325 (2024).